

Far-red photoactivatable BODIPYs for the super-resolution imaging of live cells

Yang Zhang^{a,b}, Sicheng Tang^a, Laura Ravelo^a, Janet Cusido^{a,c},
Francisco M. Raymo^{a,*}

^aLaboratory for Molecular Photonics, Department of Chemistry, University of Miami, Coral Gables, FL, United States

^bDepartment of Biomedical Engineering, Northwestern University, Evanston, IL, United States

^cDepartment of Math and Natural Sciences, Miami Dade College—Eduardo J. Padron Campus, Miami, FL, United States

*Corresponding author: e-mail address: fraymo@miami.edu

Contents

1. Introduction	2
1.1 Super-resolution imaging	2
1.2 Photoactivatable fluorophores	3
2. Equipment and materials	4
2.1 Synthesis of the photoactivatable fluorophore	4
2.2 Culture of model cell lines	9
3. Methods	10
3.1 Photochemical and photophysical characterization	10
3.2 Live-cell imaging	11
4. Analysis	12
4.1 Photochemical and photophysical characterization	12
4.2 Live-cell imaging	12
5. Notes	15
6. Summary and conclusions	16
Acknowledgment	16
References	16

Abstract

The identification of viable designs to construct switchable fluorescent probes and operate them in the interior of live cells is essential to allow the acquisition of SMLM images and permit the visualization of cellular components with sub-diffraction resolution. Our laboratories developed a mechanism to switch the fluorescence of BODIPY chromophores with the photoinduced cleavage of oxazine heterocycles under mild 405-nm illumination. With appropriate structural modifications, these switchable molecules can be engineered to immobilize covalently on large biomolecules within

lysosomal compartments of live COS-7 cells and produce bright far-red fluorescence with optimal contrast upon activation. Such a combination of properties permits the acquisition of PALM images of the labeled organelles with localization precision of *ca.* 15 nm. This article reports the experimental protocols for the synthesis of and live-cell labeling with these compounds as well as for the reconstruction of super-resolution images of the resulting biological preparations.

Abbreviations

CLSM	confocal laser-scanning microscopy
COS	CV-1 in origin with SV40 genes
EMCCD	electron-multiplying charge-coupled device
ESI	electrospray ionization
ESIMS	electrospray ionization mass spectrum
fPALM	fluorescence photoactivated localization microscopy
NMR	nuclear magnetic resonance
PALM	photoactivated localization microscopy
SMLM	single-molecule localization microscopy
TIRF	total internal reflection
TLC	thin-layer chromatography

Chemical abbreviations

BODIPY	borondipyrromethene
DCC	<i>N,N'</i> -dicyclohexylcarbodiimide
DMAP	4-dimethylaminopyridine
DMEM	Dulbecco's modified eagle medium
DMSO	dimethylsulfoxide
NHS	<i>N</i> -hydroxysuccinimide
PBS	phosphate buffer saline



1. Introduction

1.1 Super-resolution imaging

Fluorescence microscopy provides the opportunity to visualize biological samples labeled with emissive probes (Murphy, 2001). Images are acquired by exciting the probes with a laser source and collecting their emission. Both steps require the focusing of light with a lens, which in turn is accompanied by diffraction (Born & Wolf, 2002). This unavoidable physical phenomenon prevents the differentiation of features at sub-wavelength distances and

restricts the spatial resolution of conventional fluorescence images to the micrometer level. Such a stringent limitation has prevented the visualization of the many nanoscaled components governing the structure and functions of cells, until the transformative advent of super-resolution imaging (Betzig, 2015; Hell, 2015; Moerner, 2015). Seminal contributions aimed at confining fluorescence within sub-diffraction volumes (Hell & Wichmann, 1994), detecting fluorescence of single molecules (Moerner & Kador, 1989) and separating individual emitters in time (Betzig, 1995) have eventually led to a diversity of invaluable experimental schemes to reconstruct images with spatial resolution at the nanometer level. Some of them are based on the sequential localization of single molecules and are collectively termed SMLM (Li & Vaughan, 2018). The common requirement of these SMLM imaging strategies is the ability to switch the probes stochastically between emissive and non-emissive states, in order to maintain only a sparse population of fluorescent labels at any given time. Under these conditions, the probes are sequentially localized at the single-molecule level, as they interconvert between emissive and non-emissive states, to allow the gradual reconstruction of a complete image of the sample. Among the many mechanisms devised so far to switch probes between emissive and non-emissive states, those based on photoinduced transformations appear to be especially promising, predominantly because the dose of photons responsible for switching state can be controlled and delivered precisely with modern optics. In fact, early implementations of SMLM, termed PALM (Betzig et al., 2006) or fPALM (Hess, Girirajan, & Mason, 2006), were based on the ability to switch a nonemissive species into an emissive one under photochemical control.

1.2 Photoactivatable fluorophores

Photoactivatable fluorophores switch from a non-emissive to an emissive state under the influence of optical stimulations (Raymo, 2013). If the emissive state is designed to be sufficiently bright for detection at the single-molecule level, the photoinduced transformations of these switchable probes can be exploited to implement PALM schemes (Raymo, 2012). Indeed, sub-diffraction images of fixed cells, immunolabeled with photoactivatable synthetic dyes, can be reconstructed conveniently on the basis of these super-resolution strategies (Sauer & Heilemann, 2017). The extension of these protocols from fixed to live cells has instead been limited so far to a few representative examples (Wang, Frei, Salim, & Johnsson, 2019).

The relatively short wavelengths required for photoactivation, together with the inherent challenge in labeling live cells, complicate significantly the acquisition of PALM images of live samples with photoactivatable synthetic dyes. Our laboratories developed a new family of photoactivatable fluorophores with photochemical and photophysical properties that might overcome these stringent complications (Zhang, Tang, Thapaliya, Sansalone, & Raymo, 2018). They are based on the established photochemistry of *ortho*-nitrobenzyl photocages and the outstanding photophysics of BODIPY chromophores. In particular, the photoinduced conversion of **1** into **2** and **3** (Fig. 1) was specifically designed to permit the acquisition of PALM images of the lysosomal compartments of live cells (Zhang, Song, et al., 2018). This chapter describes the experimental procedures for the synthesis of these compounds as well as methods for their spectroscopic characterization, introduction in live cells and reconstruction of sub-diffraction images of the resulting preparations.



2. Equipment and materials

2.1 Synthesis of the photoactivatable fluorophore

A detailed description of the synthetic procedure and characterization can be found in the supplementary section of Zhang, Song, et al. (2018). The target photoactivatable fluorophore (**1** in Fig. 1) was synthesized in two steps from known precursors (**4** and **6**). Compound **4** was prepared following the synthetic procedure reported in Zhang, Tang, Sansalone, Baker, and Raymo (2016). Compound **6** was prepared following the synthetic procedure reported in Zhang et al. (2015). Condensation of **4** with benzaldehyde, in the presence of piperidine and acetic acid, connects a styryl substituent to the BODIPY chromophore to produce **5** (Fig. 2). Condensation of **5** and **6** fuses a *2H,4H*-benzo[1,3]oxazine heterocycle on the [C–N] bond of the *3H*-indole appendage. Treatment of the resulting intermediate with NHS, DCC and DMAP converts its carboxylic acid group into a NHS ester.

2.1.1 Equipment

1. Fume hood
2. Balance
3. Stirring hot plate
4. Round bottom flask
5. Stirbar
6. Dean-Stark apparatus

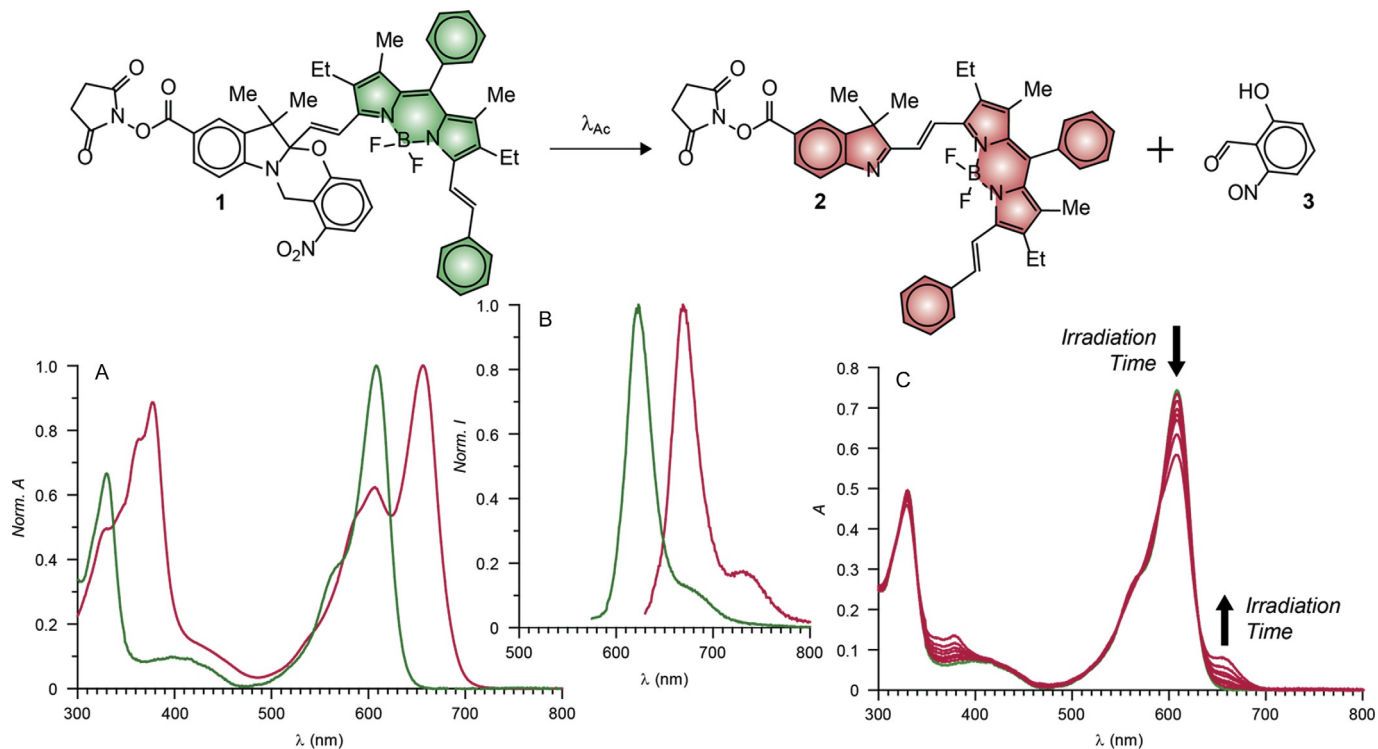


Fig. 1 Photoinduced conversion of **1** into **2**. (A) Normalized absorption spectra of **1** and **2** in THF at 25 °C. (B) Normalized emission spectra of **1** ($\lambda_{Ex} = 565$ nm) and **2** ($\lambda_{Ex} = 620$ nm) in THF at 25 °C. (C) Absorption spectra of a THF solution of **1** (10 μ M) recorded before and during irradiation (350 nm, 4.2 mW cm⁻², 10 min).

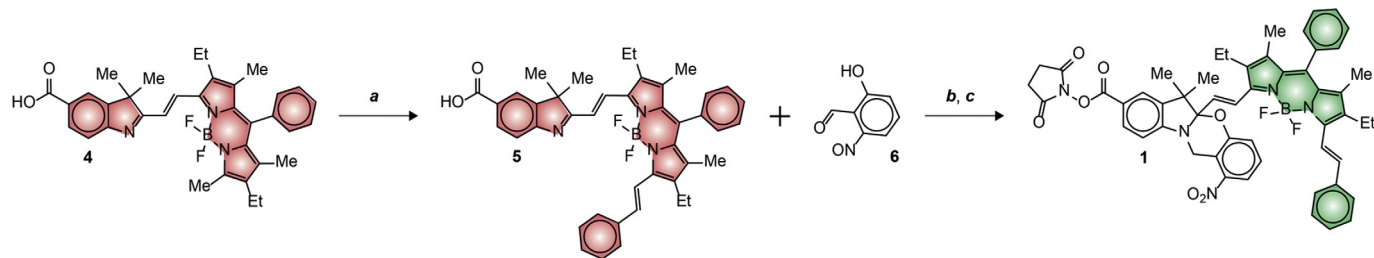


Fig. 2 Synthesis of **1**. *Reagents and conditions:* (A) piperidine, acetic acid, toluene, reflux, 24 h; (B) acetonitrile, reflux 12 h; (C) NHS, DCC, DMAP, ambient temperature, 2 h.

7. Condenser
8. Syringe
9. Rotary Evaporator
10. Separatory Funnel
11. Funnel
12. Conical flask
13. Chromatography Column
14. TLC Chamber
15. Vacuum Pump
16. ESI mass spectrometer
17. NMR tube
18. NMR spectrometer

2.1.2 Materials

1. Benzaldehyde
2. Piperidine
3. Acetic acid
4. Toluene
5. Ethyl acetate
6. Sodium bicarbonate
7. Sodium sulfate
8. Filter paper
9. Hexanes
10. Silica
11. Vials
12. TLC plates
13. Chloroform- d_3
14. Acetonitrile
15. Dichloromethane
16. NHS
17. DCC
18. DMAP
19. Acetone- d_6
20. Argon
21. Aluminum foil

2.1.3 Procedures

- (a) A solution of **4** (390 mg, 0.7 mmol), benzaldehyde (106 mg, 1.0 mmol), piperidine (0.9 mL, 9.1 mmol), acetic acid (0.6 mL, 10.5 mmol) in toluene (100 mL) was heated under reflux for 24 h in a Dean–Stark apparatus.

- (b) After cooling down to ambient temperature, the solvent was distilled off with a rotary evaporator. The residue was dissolved in ethyl acetate (50 mL) and washed with a saturated aqueous solution of sodium bicarbonate (3×30 mL). The organic layer was dried over sodium sulfate and the solvent was distilled off under reduced pressure. The residue was purified by column chromatography [silica, hexanes/ethyl acetate (3:1, v/v)] and dried under vacuum to give **5** (340 mg, 76%) as a dark-green solid.
- (c) The solid was analyzed by ESI mass spectrometry and ^1H NMR spectroscopy to confirm its structural identity. ESIMS: $m/z = 667.3233$ for $[\text{M} + \text{H}]^+$ (m/z calcd. for $\text{C}_{42}\text{H}_{41}\text{BF}_2\text{N}_3\text{O}_2 = 668.3260$); ^1H NMR (chloroform- d_3): $\delta = 8.62$ (1H, s), 8.38 (1H, d, 18 Hz), 8.10–8.05 (3H, m), 7.94 (1H, d, 16 Hz), 7.81 (2H, d, 8 Hz), 7.66–7.61 (3H, m), 7.53–7.50 (2H, m), 7.48 (1H, s), 7.45 (1H, s), 7.40–7.38 (1H, m), 7.35 (1H, d, 18 Hz), 2.71 (2H, q, 8 Hz), 2.41 (2H, q, 8 Hz), 1.60 (3H, s), 1.44 (3H, s), 1.39 (3H, s), 1.38 (3H, s), 1.17 (3H, t, 8 Hz), 1.03 (3H, t, 8 Hz).
- (d) A solution of **5** (340 mg, 0.5 mmol) and **6** (230 mg, 1.0 mmol) in acetonitrile (50 mL) was heated under reflux for 12 h.
- (e) The solvent was distilled off with a rotary evaporator and the residue was dissolved in dichloromethane (50 mL). After the addition of (115 mg, 1.0 mmol), DCC (210 mg, 1.0 mmol) and DMAP (122 mg, 1.0 mmol), the mixture was stirred at ambient temperature for 2 h.
- (f) The resulting precipitate was filtered off and the filtrate was concentrated with a rotary evaporator. The residue was purified by column chromatography [silica, hexanes/ethyl acetate (2:1, v/v)] and dried under vacuum to give **1** (67 mg, 14%) as a purple solid.
- (g) The solid was analyzed by ESI mass spectrometry and ^1H NMR spectroscopy to confirm its structural identity. ESIMS: $m/z = 916.3673$ $[\text{M} + \text{H}]^+$ (m/z calcd. for $\text{C}_{53}\text{H}_{49}\text{BF}_2\text{N}_5\text{O}_7 = 916.3693$); ^1H NMR (acetone- d_6): $\delta = 7.79$ –7.68 (4H, m), 7.67–7.58 (3H, m), 7.52 (2H, t, 8 Hz), 7.48–7.38 (5H, m), 7.37–7.34 (1H, m), 7.34–7.30 (1H, m), 7.20 (1H, dd, 2 and Hz), 6.92 (1H, d, 8 Hz), 6.80 (1H, s), 6.68 (1H, d, 17 Hz), 5.26 (1H, d, 19 Hz), 5.00 (1H, d, 19 Hz), 3.51 (4H, s), 2.69 (2H, q, 8 Hz), 2.50 (2H, q, 8 Hz), 1.68 (3H, s), 1.39 (3H, s), 1.37 (3H, s), 1.35 (3H, s), 1.16 (3H, t, 8 Hz), 0.99 (3H, t, 8 Hz).
- (h) A solution of **5** (100 mg, 0.2 mmol), NHS (23 mg, 0.2 mmol), DCC (42 mg, 0.2 mmol) and DMAP (4 mg, 0.03 mmol) in dichloromethane (50 mL) was stirred at ambient temperature for 2 h.

- (i) The resulting precipitate was filtered off and the filtrate was concentrated with a rotary evaporator. The residue was purified by column chromatography [silica, hexanes/ethyl acetate (2:1, v/v)] and dried under vacuum to give **2** (70 mg, 61%) as a dark-green solid.
- (j) The solid was analyzed by ESI mass spectrometry and ^1H NMR spectroscopy to confirm its structural identify. ESIMS: $m/z = 765.3402$ $[\text{M} + \text{H}]^+$ (m/z calcd. for $\text{C}_{46}\text{H}_{44}\text{BF}_2\text{N}_4\text{O}_4 = 765.3424$); ^1H NMR (acetone- d_6): $\delta = 8.38$ (1H, d, 17 Hz), 7.89 (1H, d, 17 Hz), 7.72 (2H, d, 7 Hz), 7.68–7.60 (4H, m), 7.54–7.48 (4H, m), 7.42 (2H, t, 8 Hz), 7.30 (2H, d, 17 Hz), 6.80 (1H, s), 3.08 (4H, s), 2.77–2.70 (4H, m), 1.59 (6H, s), 1.44 (3H, s), 1.42 (3H, s), 1.20 (6H, td, 5 and 8 Hz).
- (k) The isolated compounds were stored in the refrigerator in sealed vials under an argon atmosphere coated with aluminum foil to prevent exposure to light.

2.2 Culture of model cell lines

A detailed description of the culture, labeling and imaging of COS-7 cells can be found in the supplementary section of [Zhang, Song, et al. \(2018\)](#).

2.2.1 Equipment

1. Biosafety Cabinet
2. Incubator
3. Micropipettes
4. Coverglass

2.2.2 Materials

1. DMEM
2. L-Glutamine
3. Fetal bovine serum
4. Penicillin-streptomycin
5. Carbon dioxide
6. PBS
7. LysoTrackerTM Green DND-26
8. MitoTracker FM9
9. SYTO-13
10. DMSO

2.2.3 Procedures

- (a) COS-7 cells were grown in DMEM supplemented with L-glutamine (2 mM), fetal bovine serum (10% v/v) and penicillin-streptomycin (1% v/v, 100 U mL⁻¹) at 37 °C with carbon dioxide (5%).
- (b) The cells were plated on No. 1 borosilicate bottom 8-well coverglass with low confluency.
- (c) The cultured cells were co-incubated with **1** (1 μM, PBS) and LysoTrackerTM Green DND-26, MitoTracker FM or SYTO-13 (1 μM, PBS) for 1 h, washed with pre-warmed PBS three times and transferred on the stage of a fluorescence microscope for CLSM imaging.
- (d) A DMSO solution of **1** (100 μM) was diluted with PBS to a final concentration of 0.5 μM immediately before use. The cultured cells were incubated with the resulting solution for 1 h and rinsed with pre-warmed cell culture medium (no phenol red) three times and transferred on the stage of an optical microscope for single-molecule imaging.



3. Methods

3.1 Photochemical and photophysical characterization

A detailed description of the spectroscopic characterization of **1** and **2** can be found in the supplementary section of [Zhang, Song, et al. \(2018\)](#).

3.1.1 Equipment

1. Quartz cells
2. Photoreactor
3. Absorption spectrometer
4. Emission spectrometer

3.1.2 Materials

1. THF
2. Ethanol
3. Cresyl violet acetate
4. Oxazine 1 perchlorate
5. Potassium ferrioxalate

3.1.3 Procedures

- (a) An aerated solution of **1** (10 μM) in THF at 25 °C was irradiated in the chamber of a photoreactor (350 nm, 4.2 mW cm⁻²) for 10 min.

- (b) Absorption and emission spectra of the solution were recorded before and during irradiation at time intervals of 1 min.
- (c) Absorption and emission spectra of an aerated solution of **2** (10 μM) in THF were recorded under the same conditions.
- (d) Fluorescence quantum yields of **1** and **2** were determined against ethanol solutions of either the acetate salt of Cresyl Violet ($\phi_{\text{F}} = 0.54$) or the perchlorate salt of Oxazine 1 ($\phi_{\text{F}} = 0.15$), following the protocol reported in [Wurth, Grabolle, Pauli, Spieles, and Resch-Genger \(2013\)](#).
- (e) The quantum yield for the photochemical conversion of **1** into **2** were determined against a potassium ferrioxalate actinometer, following the protocol reported in [Scaiano \(1989\)](#).

3.2 Live-cell imaging

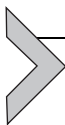
A detailed description of the experimental protocol for the imaging of live COS-7 cells labeled with **1** can be found in the supplementary section of [Zhang, Song, et al. \(2018\)](#).

3.2.1 Equipment

1. CLSM
2. TIRF objective
3. Filter sets
4. EMCCD camera

3.2.2 Procedures

- (a) CLSM images of live COS-7 cells were acquired with detection between 575 and 650 nm, under excitation at 561 nm, to collect the fluorescence of **1** and between 500 and 550 nm, under excitation at 488 nm, to collect the fluorescence of the lysosomal, mitochondrial or nuclear stain.
- (b) Epi-fluorescence images of live COS-7 cells were collected with a TIRF objective (1.49 numerical aperture) and a Cy3 filter set on an EMCCD camera, under 532-nm excitation (10 W cm^{-2}).
- (c) PALM images of cells labeled with **1** were collected with a TIRF objective (1.49 numerical aperture) and a Cy5 filter set on an EMCCD camera, under 642-nm excitation (4 kW cm^{-2}) and 405-nm activation (ramping from 0.1 to 10 W cm^{-2}) at an exposure time of 20 ms for 10,000 frames.



4. Analysis

4.1 Photochemical and photophysical characterization

The absorption and emission spectra (A and B in Fig. 1) of aerated solutions of **1** in THF show bands with maxima at 608 and 623 nm respectively for the BODIPY chromophore. The molar absorption coefficient (ϵ) and fluorescence quantum yield (ϕ_F) are $74.7 \text{ mM}^{-1} \text{ cm}^{-1}$ and 0.89, respectively. These values correspond to a brightness ($\epsilon \times \phi_F$) of $66 \text{ mM}^{-1} \text{ cm}^{-1}$. Under ultraviolet irradiation, the *ortho*-nitrobenzyl component of **1** cleaves irreversibly to produce **2** and **3**. This structural transformation extends the electronic delocalization of the BODIPY chromophore over a 3*H*-indole auxochrome. As a result, the absorption and emission bands of the BODIPY chromophore of **2** shift to 656 and 669 nm respectively (A and B in Fig. 1). The values of ϵ , ϕ_F and $\epsilon \times \phi_F$ for **2** are $76.8 \text{ mM}^{-1} \text{ cm}^{-1}$, 0.40 and $30 \text{ mM}^{-1} \text{ cm}^{-1}$, respectively. Absorption spectra (C in Fig. 1), recorded over the course of the photolytic transformation of **1** into **2**, show a gradual decrease in the band of the former with the concomitant appearance and growth of that of the latter. The quantum yield of this photochemical process is 0.009.

4.2 Live-cell imaging

CLSM images (A, D and G in Fig. 3) of live COS-7 cells co-incubated with **1** and a lysosomal, mitochondrial or nuclear stain show the characteristic BODIPY fluorescence between 575 and 650 nm in the intracellular environment upon excitation at 561 nm. Detection between 500 and 550 nm, upon excitation at 488 nm, also reveal the fluorescence of the co-stains in the intracellular environment (B, E and H in Fig. 3). Overlays of the two detection channels (C, F and I in Fig. 3), however, show co-localization of **1** exclusively with the lysosomal stain. The corresponding Pearson's coefficient is 0.98.

Mild illumination of live COS-7 cells labeled with **1** at 405 nm generates a sparse population of **2** in the lysosomal compartments. Selective excitation of the photochemical product at 642 nm allows the localization of the few activated molecules with nanoscaled precision and their subsequent bleaching. As a result, the reiterative activation and bleaching of sub-populations of **1** and **2** respectively enable the reconstruction of sub-diffraction images

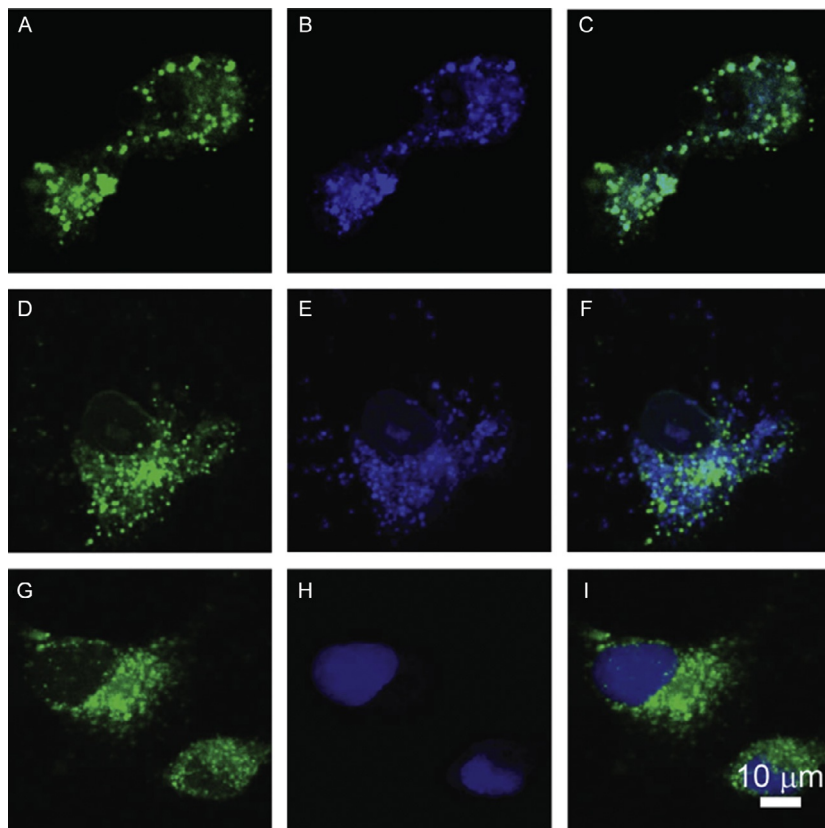


Fig. 3 CLSM imaging of live COS-7 cells. (A–C) Cells co-incubated with **1** (green) and a lysosomal stain (blue). (D–F) Cells co-incubated with **1** (green) and a mitochondrial stain (blue). (G–I) Cells co-incubated with **1** (green) and a nuclear stain (blue). *Adapted with permission from Zhang, Y., Song, K.-H., Tang, S., Ravelo, L., Cusido, J., Sun, C., et al., (2018). Far-red photoactivatable BODIPYs for the super-resolution imaging of live cells. Journal of the American Chemical Society, 140(40), 12741–12745. Copyright (2019) American Chemical Society.*

(A–C in Fig. 4) of the labeled lysosomes, which instead cannot be resolved in the corresponding diffraction-limited epi-fluorescence image (inset) of the very same sample. The intensity trajectory (D in Fig. 4) of the activation/bleaching process from a 7×7 pixel area shows distinct intensity spikes over the entire acquisition time. The line profiles of the green- and blue-highlighted regions indicate the size of individual lysosomes to be *ca.* 80 nm (E in Fig. 4). The localization precision is *ca.* 15 nm with a mean photon count of *ca.* 2000 (F and G in Fig. 4).

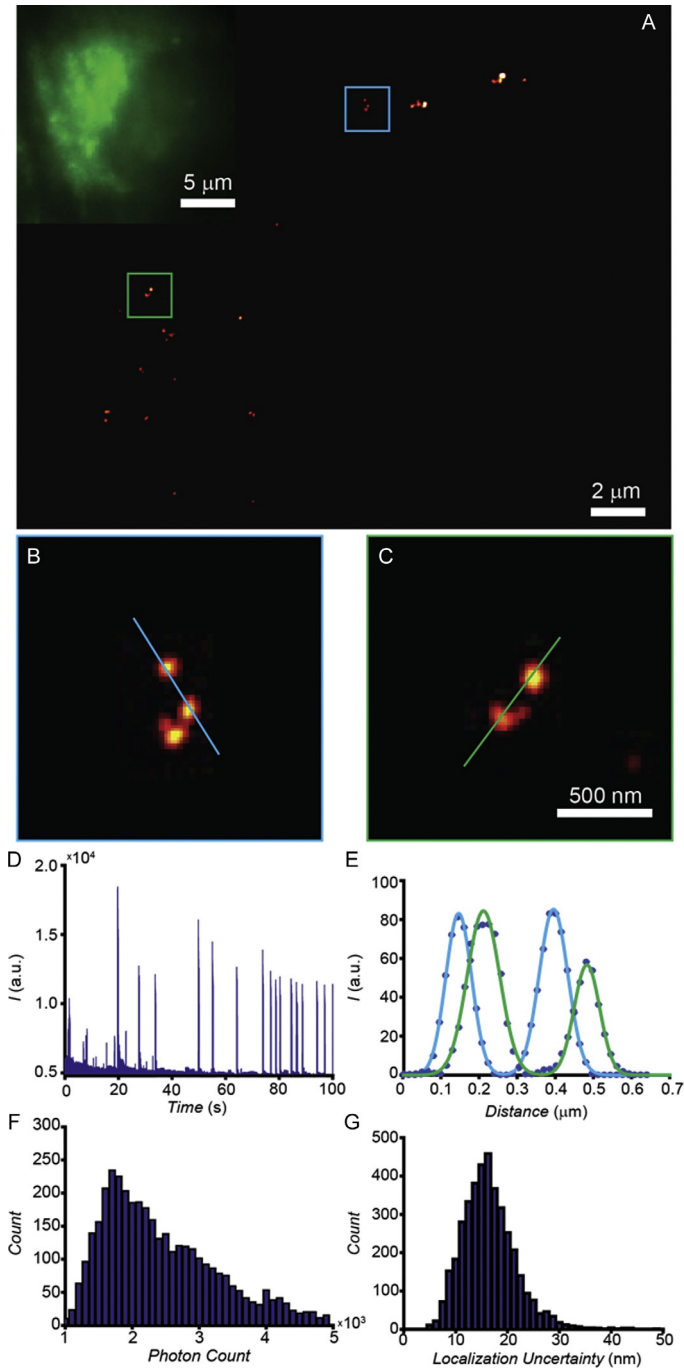


Fig. 4 See figure legend on opposite page.



5. Notes

- (1) Chemicals were purchased from commercial sources and used as received with the exception of acetonitrile, dichloromethane and THF. The former two solvents were distilled over calcium hydride. The latter was distilled over sodium and benzophenone.
- (2) EISMS were recorded with a Bruker micrOTO-Q II spectrometer.
- (3) ^1H NMR spectra were recorded with a Bruker Avance 400 spectrometer.
- (4) Absorption spectra were recorded with a Varian Cary 100 Bio spectrometer in quartz cells with a path length of 1.0 cm.
- (5) Emission spectra were recorded with a Varian Cary Eclipse spectrometer.
- (6) Photolysis was performed with a Luzchem Research LZC-4V photoreactor.
- (7) Diffraction-limited images were recorded with a Leica SP5 CLSM.
- (8) PALM and epi-fluorescence images were acquired with a Nikon Ti-E inverted microscope equipped with a Nikon CFI Apochromat TIRF objective, Semrock Cy3 and Cy5 filter sets, an Andor iXon 897 EMCCD camera and continuous-wave Spectra Physics Excelsior One lasers.
- (9) All experiments were performed ensuring minimal exposure of the photosensitive probe to ambient light.
- (10) The NHS ester in position 5 of the 3*H*-indole heterocycle of **1** ensures the covalent connection of the photoactivatable probes to primary amino groups of intracellular proteins. Covalent connection of the probe to relatively large biomolecules restricts diffusion sufficiently to allow the sequential localization of single molecules with nanoscaled precision required to reconstruct PALM images. Negligible diffusion

Fig. 4 Super-resolution imaging of live COS-7 cell. (A) PALM and epi-fluorescence (inset) images of a cell labeled with **1**. (B and C) Magnifications of the highlighted regions. (D) Representative single-molecule blinking trajectory, recorded within a 7×7 pixel area in the same sample after photoactivation. (E) Line measurements with Gaussian fitting of individual lysosomes in **b** and **c**. (F) Photon count of the single-molecule photoactivation events. (G) Localization uncertainty parameters of the single-molecule photoactivation events. *Adapted with permission from Zhang, Y., Song, K.-H., Tang, S., Ravelo, L., Cusido, J., Sun, C., et al., (2018). Far-red photoactivatable BODIPYs for the super-resolution imaging of live cells. Journal of the American Chemical Society, 140(40), 12741 – 12745. Copyright (2019) American Chemical Society.*

was confirmed by tracking the spatial coordinates of single molecules of **2** in the lysosomal compartments for tens of milliseconds as reported in Zhang, Song, et al. (2018).



6. Summary and conclusions

The photoinduced and irreversible cleavage of an oxazine heterocycle can be exploited to bring a BODIPY chromophore in electronic conjugation with a 3*H*-indole auxochrome. Such a pronounced structural transformation shifts bathochromically the absorption band of the chromophore to allow the selective excitation of the photochemical product with concomitant bright fluorescence in the red region of the electromagnetic spectrum. These photochemical transformations can be reproduced in the intracellular environment of live cells under illumination with lasers lines at 405 and 642 nm for activation and localization, respectively. Specifically, the photoactivatable probes enter the lysosomal compartments of the live cells, where they can be activated, localized at the single-molecule level and bleached stochastically. Reiteration of this sequence of events permits the reconstruction of PALM images of the labeled organelles with localization precision of *ca.* 15 nm. Thus, the photochemical, photophysical and structural properties engineered into this particular photoactivatable fluorophore provide the rare opportunity to image subcellular structures of live cells with sub-diffraction resolution.

Acknowledgment

The National Science Foundation (CHE-1505885) is acknowledged for financial support.

References

- Betzig, E. (1995). Proposed method for molecular optical imaging. *Optics Letters*, 20(3), 237–239.
- Betzig, E. (2015). Single molecules, cells and super-resolution optics. *Angewandte Chemie International Edition*, 54(28), 8034–8053.
- Betzig, E., Patterson, G. H., Sougrat, R., Lindwasser, O. W., Olenych, S., Bonifacino, J. S., et al. (2006). Imaging intracellular fluorescent proteins at nanometer resolution. *Science*, 313(5793), 1642–1645.
- Born, M., & Wolf, E. (2002). *Principles of optics*. Cambridge: Cambridge University Press.
- Hell, S. W. (2015). Nanoscopy with focused light. *Angewandte Chemie International Edition*, 54(28), 8054–8066.
- Hell, S. W., & Wichmann, J. (1994). Breaking the diffraction resolution limit by stimulated emission: Stimulated-emission-depletion fluorescence microscopy. *Optics Letters*, 19(11), 780–782.

- Hess, S. T., Girirajan, T. P. K., & Mason, M. D. (2006). Ultra-high resolution imaging by fluorescence photoactivation localization microscopy. *Biophysical Journal*, *91*(11), 4258–4272.
- Li, H., & Vaughan, J. C. (2018). Switchable fluorophores for single-molecule localization microscopy. *Chemical Reviews*, *118*(18), 9412–9454.
- Moerner, W. E. (2015). Single-molecule spectroscopy, imaging and photocontrol: Foundations for super-resolution microscopy. *Angewandte Chemie International Edition*, *54*(28), 8067–8093.
- Moerner, W. E., & Kador, L. (1989). Optical detection and spectroscopy of single molecules in a solid. *Physical Review Letters*, *62*(21), 2535–2538.
- Murphy, D. B. (2001). *Fundamentals of light microscopy and electronic imaging*. New York: Wiley-Liss.
- Raymo, F. M. (2012). Photoactivatable synthetic dyes for fluorescence imaging at the nanoscale. *Journal of Physical Chemistry Letters*, *3*(17), 2379–2385.
- Raymo, F. M. (2013). Photoactivatable synthetic fluorophores. *Physical Chemistry Chemical Physics*, *15*(36), 14840–14850.
- Sauer, M., & Heilemann, M. (2017). Single-molecule localization microscopy in eukaryotes. *Chemical Reviews*, *117*(11), 7478–7509.
- Scaiano, J. C. (1989). *Handbook of organic photochemistry*. Boca Raton: CRC Press.
- Wang, L., Frei, M. S., Salim, A., & Johnsson, K. (2019). Small-molecule fluorescent probes for live-cell super-resolution microscopy. *Journal of the American Chemical Society*, *141*(7), 2770–2781.
- Wurth, C., Grabolle, M., Pauli, J., Spieles, M., & Resch-Genger, U. (2013). Relative and absolute determination of fluorescence quantum yields of transparent samples. *Nature Protocols*, *8*(8), 1535–1550.
- Zhang, Y., Song, K.-H., Tang, S., Ravelo, L., Cusido, J., Sun, C., et al. (2018). Far-red photoactivatable BODIPYs for the super-resolution imaging of live cells. *Journal of the American Chemical Society*, *140*(40), 12741–12745.
- Zhang, Y., Swaminathan, S., Tang, S., Garcia-Amorós, J., Boulina, M., Captain, B., et al. (2015). Photoactivatable BODIPYs designed to monitor the dynamics of supramolecular nanocarriers. *Journal of the American Chemical Society*, *137*(14), 4709–4719.
- Zhang, Y., Tang, S., Sansalone, L., Baker, J. D., & Raymo, F. M. (2016). A photoswitchable fluorophore for the real-time monitoring of dynamic events in living organisms. *Chemistry—A European Journal*, *22*(42), 15027–15034.
- Zhang, Y., Tang, S., Thapaliya, E. R., Sansalone, L., & Raymo, F. M. (2018). Fluorescence activation with switchable oxazines. *Chemical Communications*, *54*(64), 8799–8809.